Jurnal Teknologi

Full Paper

ANALYSIS OF GLOBAL AND LOCAL MAXIMUM POWER POINTS IN PV ARRAYS UNDER PARTIAL SHADING CONDITION

Bambang Mulyo Raharjo*

Electrical Engineering, Sekolah Tinggi Teknologi Duta Bangsa, Bekasi, Indonesia

Article history
Received
1 January 2023
Received in revised form
18 March 2023
Accepted
4 April 2023
Published Online
25 June 2023

*Corresponding author
bambang.mulyo@sttdb.ac.id

Graphical abstract

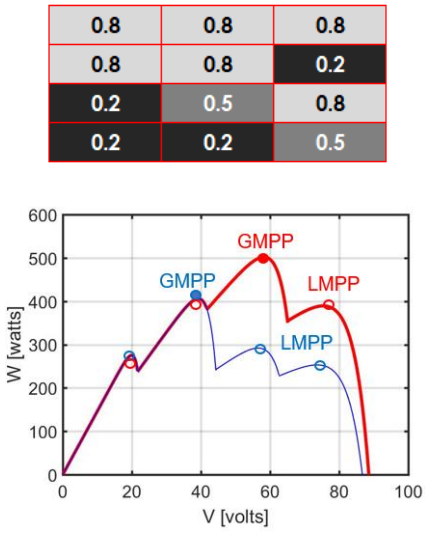

Abstract

Partial shading (PS) has a significant impact on the decrease in efficiency of photovoltaic (PV) array and performance of maximum power point tracking (MPPT) that must be addressed. We conduct an analysis and evaluation of local maximum power point (LMPP) in terms of quantity, and global maximum power point (GMPP) in terms of magnitude and diversity. Simulation is carried out using single diode ideal model and nine generic PS patterns that are specifically designed to bring up the substantial characteristics of the LMPP and GMPP and applied to series-parallel (SP) and total cross-tied (TCT) configurations. The SP configuration has LMPP with two, three, and four peaks, appearing three times each. The TCT configuration has two peaks that appear six times, three peaks that appear once, and four peaks that appear twice. The SP configuration experiences power losses ranging from 56% to 72%, while the TCT configuration has power losses ranging from 52% to 64%. The SP configuration generates a maximum voltage of 76.64 volts and a minimum of 39.20 volts, while the TCT configuration generates a maximum voltage of 77.62 volts and a minimum of 58.21 volts. With a smaller number of LMPP, a larger magnitude of GMPP parameters, and lower diversity, TCT exhibits better characteristics and performance compared to SP.

Keywords: PV array, series-parallel configuration, total cross-tied configuration, partial shading, local maximum power point, global maximum power point

1.0 INTRODUCTION

Nowadays solar panel system power plants are one of the most suppliers of renewable electrical energy which is already being used in a mass compared to other renewable energy sources. In addition to being derived from abundant and eco-friendly solar sources, the low costs of operation and maintenance, as well as the ease of construction, render it a promising prospect for future access to renewable electrical energy worldwide [1], [2]. In recent years, solar panel technology has become popular with a total installed power of 627 GW in 2019 and in some reports predicting growth of 46% by 2023 [3], [4]. Solar panel electrical energy is produced from the direct transformation of solar radiation, where this energy conversion is conducted using PV cells based on a physical phenomenon known as the photovoltaic effect [5]. PV cells generates a potential difference and become a source of electric current when the surface of this cell is exposed to the sunlight [6].

The performance of PV cells is determined by internal and external parameters. The main influence of external factors is solar irradiation and surface temperature of the PV cells [7], [8]. The influence of internal parameters such as photogenerated current,

reverse saturation current, and ideality factor distinguishes the performance of one PV cell from another. The parasitic resistances of the PV cell are involved in the calculations, causing power losses in practical PV modules [9]–[11]. A good PV cell must have a small series resistance and a large parallel resistance value to approach ideal conditions.

To obtain the desired output voltage and power, solar panel system power plants are usually developed by forming a configuration of PV modules known as arrays [12], [13]. The PV module itself is built from a series-parallel connection of PV cells. Configurations of arrays connection that are often used include series-parallel (SP), total cross-tied (TCT), bridge-linked (BL), and honeycomb (HC) [14], [15]. This configuration is primarily to address the potential of PS occurring on the surface of the solar panel arrays. The PS condition occurs when the solar panel cannot fully receive sunlight irradiation due to the partial covering of its surface by the shadow of objects such as buildings, trees, as well as the clouds. PS condition causes a drastic decrease in the output power of the solar panel system, thereby reducing efficiency and changing the maximum power point tracking (MPPT) algorithm [16]–[18].

Several ways and methods are applied to overcome PS conditions with a purpose to keep the solar panel system operating at MPP. Study and research in investigating the proper PV arrays connection configuration is necessary to get an optimum performance. One practical and useful way to predict the characteristics and performance of PV arrays is by means of simulation. Simulation provides an easy and fast approach to study the characteristics of PV arrays. Such studies are often used to investigate response of PV arrays to environmental factors and to develop maximum power point tracking (MPPT) algorithms [19]–[25]. The MPPT itself involves calculating LMPP and GMPP which are the parameters that determine the performance of the PV array [16]. The only LMPP is the GMPP itself, which takes place in non-PS (NPS) conditions. So, the less the number of LMPPs, the better the performance of the PV array. The desired GMPP is one that has a voltage close to the maximum voltage in the NPS condition. Whereas GMPP with less voltage is not an option.

The main objective of our research is to complement the existing methods in analyzing and evaluating the performance of PV arrays in PS condition in more detail. The study is applied to the conventional SP and TCT as frequent and common configurations used. Our investigation includes: (i) analysis involving the characteristics of LMPP in terms of peaks number and frequency of occurrence, as well as GMPP in terms of magnitude and diversity; (ii) designing common PS patterns for simulation that can bring out the distinctiveness of both LMPP and GMPP characteristic of SP and TCT; (iii) the simulation is conducted on nine different variations of PS patterns arranged to be equal shadowed area percentages, so that the losses incurred can be directly compared. Hence, we will gain a more complete and detailed understanding of SP and TCT regarding ease of implementing MPPT. Besides that, knowing which PS patterns producing the worst, moderate, and best characteristics, and performance of PV arrays configuration.

2.0 METHODOLOGY

The configuration characteristic and performance of the PV array are thoroughly represented by LMPP and GMPP characteristics. The characteristics of LMPP are revealed through the number of peaks and their frequency of occurrence, which indicate diversity. The characteristics of GMPP, in addition to its magnitude, its diversity is also important to be identified. The situation is highly dependent on the type of operating conditions that occurs. In addition to determining the magnitude of GMPP parameters, as many previous studies have done, they also form the LMPP and GMPP topology of the PV array configuration. In this study, we use SP and TCT configurations as preliminary in developing the understanding of PV array characteristic analysis with various PS patterns. In addition, we also aim to examine the differences between the two configurations in more depth and detail. For this purpose, MATLAB simulation uses an ideal single diode model that is low-cost and requires minimal resources yet is sufficiently accurate. The parameters of LMPP and GMPP are obtained by calculating mathematical equations derived from the model.

2.1 Mathematical Modelling

A single diode circuit representing an ideal PV cell excluding parasitic resistances is used as the basis for providing a mathematical model of the SP and TCT configurations. This is to reduce the complexity of mathematical formulas that affect computational numerical iterations. The current-voltage equation of the PV cell is given as follows [19], [26]:

$$\left.\begin{aligned} I &= I_{ph} - I_D \\ I_D &= I_o\left[exp\left(\frac{qV}{AkT}\right) - 1\right] \\ I_{ph} &= \delta[I_{sc} - C_t(T - T_o)] \\ I_o &= I_{so}\left(\frac{T}{T_o}\right)^3 exp\left[\frac{qE_g}{Ak}\left(\frac{1}{T_o} - \frac{1}{T}\right)\right], \end{aligned}\right\} \quad (1)$$

where I and V are the output current and voltage of PV cell, respectively. I_{ph}, I_D, I_o, I_{so}, I_{sc} are the photo-generated current, diode current, dark saturation current, diode saturation current, and short circuit current of PV cell, respectively. T, T_o, E_g, A, C_t, q, and k are the ambient temperature, standard test temperature, bandgap, ideality factor, temperature coefficient, electronic charge, and Boltzmann constant, respectively. The $\delta = S/S_o$ is the ratio of actual and standard test irradiances (S_o = 1000 watt/m^2, T_o = 25 °C).

An electrical circuit analysis of the ideal PV array is based on Figure 1, which explains the series and parallel connection of the identical PV modules at the same irradiation value. Due to the existence of current sources in series connection, the occurrence of local overheating of modules in PS condition can be avoided by connecting them through the external bypass diodes [27]. The total photo-generated current in series connection is generally taken as the minimum value expressed as:

$$I_{ph,s} = \min\left[I_{ph,i}\right]_{i=1}^{N_s}, \tag{2}$$

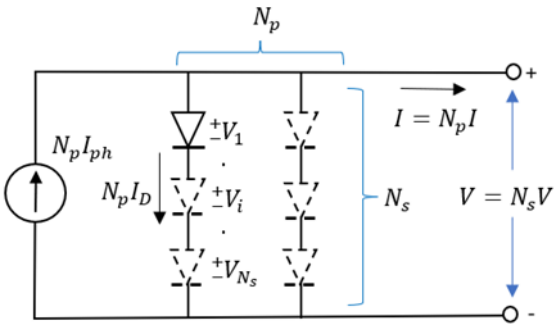

Figure 1 Equivalent circuit of ideal PV arrays

where *i and* N_s are the number of the i^{th} PV module and the total number of PV modules connected in series, respectively. If the PV cells are identical and the temperature of each PV module are considered equal, so by using the irradiance ratio δ, Equation (2) can be rewritten as:

$$I_{ph,s} = I_{ph} \cdot \min\left[\delta_i\right]_{i=1}^{N_s}. \tag{3}$$

The total voltage is $V_s = V_1 + V_2 + \ldots + V_j + \ldots + V_{NS}$, and the diode current in the series connection for identical modules can also be written as Equation (1), $I_{D,s} = I_D$. Hence, the total current in series connection is:

$$I_s = I_{ph,s} - I_{D,s}. \tag{4}$$

In a parallel connection, the PV module voltages are $V_1 = V_2 = \ldots = V_j = \ldots = V_{Np} = V_p$, and the total photo-generated current is the sum of the currents of each PV module as follows:

$$I_{ph,p} = I_{ph} \sum_{j=1}^{N_p} \delta_j. \tag{5}$$

On the other hand, the total diode current is given by the Equation:

$$I_{D,p} = I_o \sum_{j=1}^{N_p} \left[exp\left(\frac{qV_p}{AkT}\right) - 1\right]. \tag{6}$$

So, if each PV module are identical, Equation (7) can be rewritten as:

$$I_{D,p} = N_p I_o \left[exp\left(\frac{qV_p}{AkT}\right) - 1\right], \tag{7}$$

where *j* and N_p are the number of the j^{th} PV module and the total number of PV modules connected in parallel, repectively. The total current in parallel connection is:

$$I_p = I_{ph,p} - I_{D,p} \tag{8}$$

The SP and TCT configurations equipped with bypass diodes are shown in Figure 2 (a) and (b), respectively. Both SP and TCT configurations are built from PV module in series-parallel connections forming rows and columns. The bypass-diode is used to bypass the module's current in PS conditions.

In deriving mathematical model of SP configuration, the first step is to connect the number of PV modules in series for each column. Using Equation (3), the photo-generated current in the i^{th} series connection of the j^{th} column is:

$$I_{ph(i,j)} = I_{ph} \cdot min\left[\delta_{i,j}\right]_{i=1}^{N_s}, \tag{9}$$

and if

$$\Delta_{i,j} = min\left[\delta_{i,j}\right]_{i=1}^{N_s}, \tag{10}$$

then (9) can be written as follows:

$$I_{ph(i,j)} = I_{ph}\Delta_{i,j}. \tag{11}$$

Whereas the diode current has the same value for all columns which is given by:

$$I_{D(i,j)} = I_o \left[exp\left(\frac{qV_i}{AkT}\right) - 1\right]. \tag{12}$$

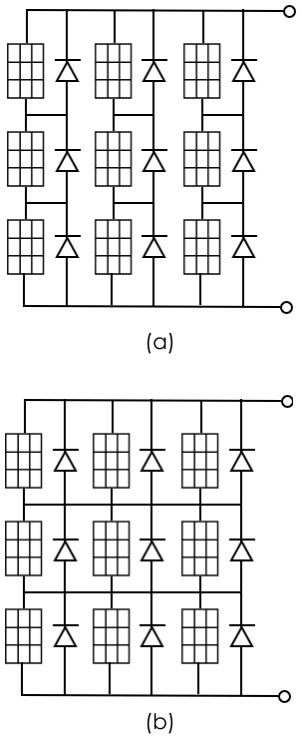

Figure 2 (a) SP and (b) TCT configuration equipped with bypass diodes

Hence, using (4) the PV current of the j^{th} column is sum of (11) an (12) yielding the following:

$$I_{PV(i,j)} = I_{ph}\Delta_{i,j} - I_o\left[exp\left(\frac{qV_i}{AkT}\right) - 1\right] \quad (13)$$

The voltage of PV modules in the i^{th} series connection is obtained by changing (13) to be:

$$V_i = \frac{AkT}{q} ln\left(\frac{I_{ph}\Delta_{i,j} - I_{PV(i,j)} + I_o}{I_o}\right) \quad (14)$$

The voltage in series connection of N_s modules for each column is then the sum of (14) as follows:

$$V_t = \frac{AkT}{q}\sum_{i}^{N_s} ln\left(\frac{I_{ph}\Delta_{i,j} - I_{PV(i,j)} + I_o}{I_o}\right) \quad (15)$$

From (14) and (15) we have:

$$V_i = V_t/i, \quad (16)$$

The second step is to connect in parallel the photogenerated current using (5) and (11) as follows:

$$I_{ph(i)} = I_{ph}\sum_{j=1}^{N_p}\Delta_{i,j}. \quad (17)$$

Using (12) and (16), the diode current is connected in parallel yielding to the equation:

$$I_{D(i)} = I_o\sum_{j=1}^{N_p}\left[exp\left(\frac{qV_t}{AkTi}\right) - 1\right] \quad (18)$$

Hence, rewriting (18) in the form of (7), and then by summing (17) and (18) for identical PV modules, the I-V characteristic for each increase of the i^{th} row is determined by the equation:

$$I = I_{ph}\sum_{j=1}^{N_p}\Delta_{i,j} - N_pI_o\left[exp\left(\frac{qV_t}{AkTi}\right) - 1\right] \quad (19)$$

The above equation is used to determine local MPP (LMPP) in which V_t reflects the output voltage of PV array. The global MPP (GMPP) current I_{GMPP} is then taken as the maximum value of the LMPP current.

The I-V equation of the TCT configuration is derived first from the parallel connection, and then connected in series for the i^{th} row. The photogenerated current is obtained by using (5) for the i^{th} row as follows:

$$I_{ph(i,j)} = I_{ph}\sum_{j=1}^{N_p}\delta_{i,j}. \quad (20)$$

To get the series-connected current magnitude, we take the smallest value of (20) and write it as in Equation (2), we get:

$$I_{ph(i)} = I_{ph}\cdot min\left[I_{ph}\sum_{j=1}^{N_p}\delta_{i,j}\right]_{i=1}^{N_s} \quad (21)$$

If we take:

$$\nabla_i = min\left[I_{ph}\sum_{j=1}^{N_p}\delta_{i,j}\right]_{i=1}^{N_s}, \quad (22)$$

Equation (21) can be simplified as:

$$I_{ph(i)} = I_{ph}\nabla_i. \quad (23)$$

By treating the identical PV module, the diode current is given by using (7) and (16) as follows:

$$I_{D,i} = N_pI_o\left[exp\left(\frac{qV_t}{AkTi}\right) - 1\right]. \quad (24)$$

Hence, the array current of TCT configuration is then the sum of (23) and (24):

$$I = I_{ph}\nabla_i - N_pI_o\left[exp\left(\frac{qV_t}{AkTi}\right) - 1\right] \quad (25)$$

As with the SP configuration, Equation (25) is used to determine both LMPP and GMPP current as well.

2.2 Partial Shading Patterns

We use PS patterns that are most likely to form on the surface of the PV array. To make a valid comparison of the LMPP and GMPP parameters for each PS pattern, the portion of the PV array surface exposed to the PS is made to be 45% of the testing standard. The PV array used for simulation has size of 4 rows and 3 columns (4x3) with the pattern of the PS experienced by 6 modules of 20%, 2 modules of 50%, and 4 modules of 80% to achieve a 45% proportion ratio. Figure 3 (a) - (i) shows the nine PS patterns which is presented by the ratio of received irradiation to the standard test $\delta_{i,j}$ in a 4x3 PV array.

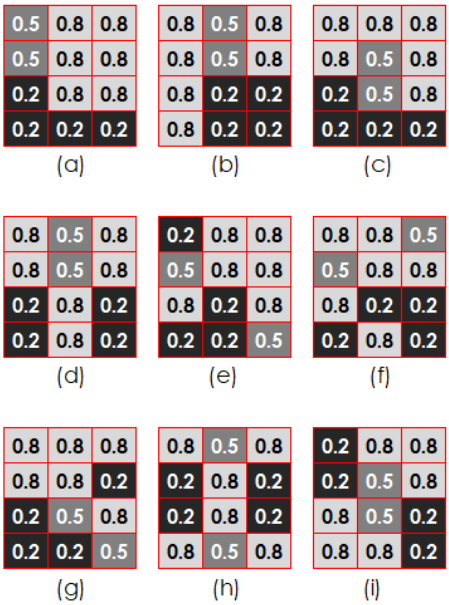

Figure 3 Partial shading patterns used for the 4x3 size PV array simulation

2.3 Computational Procedure

We utilize the conventional perturb and observe (P&O) method, which is well-known for its reliability, without emphasizing on improving the MPPT method itself. We used the P&O method to obtain the LMPP and GMPP parameters as illustrated in Figure 4. $V_{LMPP}(k)$, $I_{LMPP}(k)$,

$P_{LMPP}(k)$ are voltage, current, and power, as LMPP parameters of the PV array, respectively, in the step of k. $V_{LMPP}(k-1)$ and $P_{LMPP}(k-1)$ are voltage and power of LMPP, respectively, in the step of k-1. The constant ε denotes the perturbation voltage. On the other hand, $P_{GMPP}(k)$, $V_{GMPP}(k)$, and $I_{GMPP}(k)$ are power, voltage, and current as the parameters of GMPP of the PV arrays, respectively, in the step of k. The boxes labeled SP and TCT indicate the calculation process of LMPP and GMPP parameters using Equations (19) and (25).

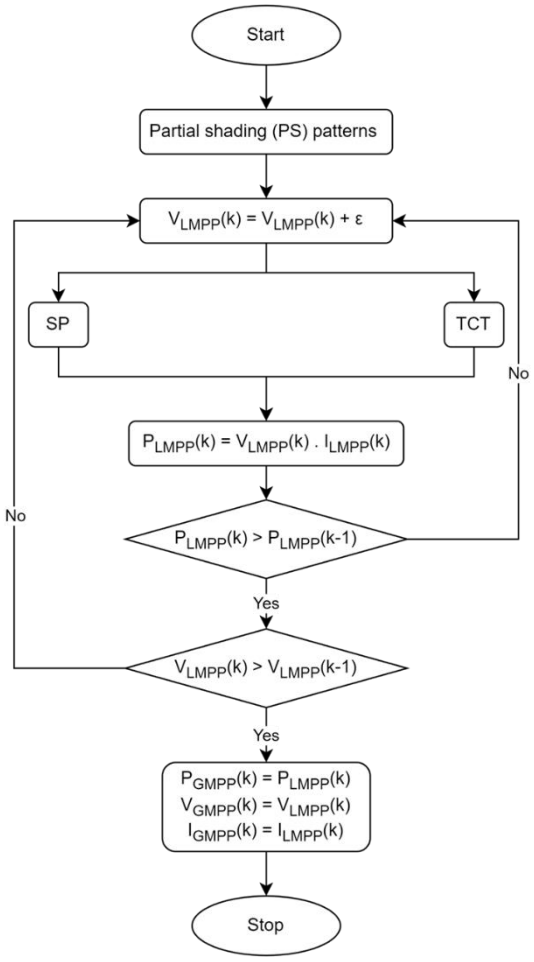

Figure 4 The flowchart shows the process of calculating the LMPP and GMPP parameters

3.0 RESULTS AND DISCUSSION

To ensure that the programming algorithm works correctly, we compare the simulation results to the previous research [28] as shown in Table 1. We tested 6x4 size arrays in two different patterns (Pat-1 and Pat-2) using Equation (19) and (25). The simulation results showed good suitability for pattern 1 produced by the SP and TCT configurations, as well as pattern 2 that provided by the TCT. Meanwhile, the SP just showed discrepancies in pattern 2 since we did not find a total current of up to 10.01 A. In the pattern 2, our simulation resulted in the highest current of just up to 6.46 A, corresponded to the maximum total current that can be generated in that pattern. The slight difference in the results is probably due to the use of different model in the calculations. We used an ideal single diode model without internal series and parallel resistances, while in [28] a two-diode model involving internal resistances was used. Here we still believe that our calculation results are correct, where in the pattern 2, it is impossible for the current generated by SP to reach the range of 10 A if we assume that several current sources are connected in series, then the total current is equal to the source with the smallest current.

Table 1 The simulation test result

	This work			Previous work		
	Pm	**Vm**	**Im**	**Pm**	**Vm**	**Im**
Pat -1						
SP	1194.2	103.50	11.54	1229.1	103.44	11.88
TCT	1194.2	103.50	11.54	1268.6	103.89	12.21
Pat-2						
SP	366.6	100.40	3.65	532.9	53.25	10.01
TCT	654.8	105.12	6.23	662.1	105.23	6.29

For simulation process in this work, we use the datasheet of the ICA100P Solar panel at the standard test of 25 °C, A.M 1.5, 1000 W/m^2 as shown in Table 2 [1]. I_m and V_m are current and voltage at P_m, respectively, whereas P_m is maximum power (MPP).

Table 2 Parameters of the KC200GT Solar Array at 25 °C, A.M 1.5, 1000 W/m^2

I_m	5.69 A
V_m	17.6 A
P_m	100 W
I_{sc}	6.09 A
V_{oc}	22.6 V
C_t	0.003958 A/K
I_{so}	$8.99 \cdot 10^{-9}$ A
A	1.25052

Figure 5 shows the I–V and P–V characteristic of the standard testing of 4x3 PV array in NPS condition using the parameters in the Table 2. The MPP shifts towards a larger value due to the ideal model excluding parasitic resistances. The PV array generates a power of 1,394 watts, a voltage of 80.68 volts, and a current of 17.28 amperes at MPP. The following simulation results for various PS pattern variations are referenced and compared to these standard parameters.

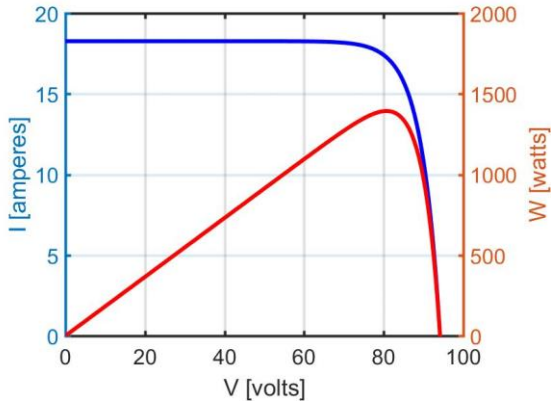

Figure 5 The I–V and P–V characteristic of the 4x3 PV array standard testing

By first converting the PS patterns into *δ* matrix form and substituting them into Equations (19) and (25), simulations are carried out and calculating the power in watts, voltage in volts, and current in amperes as GMPP parameters of the configurations for all PS patterns. Figure 6 shows the P-V characteristic curves of the SP configuration (thin blue line) and TCT configuration (thick red line) with their LMPP and GMMP using PS pattern in Figure 3(g). The empty and filled small blue circles mark the LMPP and GMPP of the SP configuration, respectively. Meanwhile, the empty and filled small red circles indicate the LMPP and GMPP of the TCT configuration, respectively. In the PS pattern, both the SP and TCT configurations have four LMPP peaks. The GMPP of the SP configuration takes place the second peak, while the GMPP of the TCT configuration can be found at the third peak.

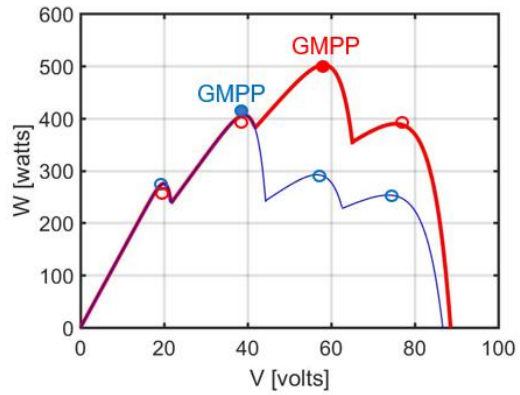

Figure 6 The P-V characteristic of SP (thin blue line) and TCT (thick red line) configurations with LMPPs and GMPPs

Table 3 shows the simulation results in the form of GMPP and LMPP parameters for both SP and TCT configurations for all PS patterns shown in Figure 3 (a) – (i). According to the simulation study, when the PS coverage on the surface of PV arrays is set to 45% of the average, the SP configuration generally incurs higher power losses in terms of GMPP than the TCT configuration across most PS patterns. Specifically, the SP configuration suffers from GMPP power losses of 56% and 72% at the lowest and highest values, respectively, while the TCT configuration experiences power losses of 52% and 64% at the lowest and highest values, respectively. Nevertheless, there are also losses shown by the SP configuration that are the same as those experienced by the TCT configuration, namely on the PS pattern in Figures 3 (a) dan (b). Apart from that, the losses experienced by the SP show a higher value compared to TCT. One interesting thing to note is that in the PS that forms a diagonal pattern, the SP configuration shows the highest losses, whereas in the TCT configuration, the pattern results in the lowest losses. The analysis also reveals that the GMPP voltages of the SP and TCT configurations vary significantly, with the SP configuration having the lowest GMPP voltage of 39.20 volts and the highest of 76.54 volts. On the other hand, the TCT configuration has the lowest GMPP voltage of 58.21 volts, and the highest of 77.62 volts. As is the case with losses, there are also voltages generated by the SP configuration that are the same as those generated by the TCT configuration on the PS pattern in Figures 3(a)-(c). The TCT configuration for PV arrays can provide a higher output voltage compared to the SP configuration under similar partial shading conditions. This is because the TCT configuration allows for a more even distribution of current among the PV modules, reducing the impact of shading on the performance of the array. In contrast, the SP configuration can result in voltage mismatches between the shaded and unshaded modules, leading to a reduced output voltage and power. As a result, the TCT configuration can provide better performance than the SP configuration in terms of output voltage and power under partial shading conditions.

Another important thing is the GMPP diversity, which is determined by how many of the same GMPPs and their frequency of occurrence. The SP configuration delivers power outputs of 608.8, 528.2, 501.9, and 477.8 watts individually, twice with 389.3 watts, and three times with 405.9 watts. The TCT configuration generates power outputs of 669.2 watts individually, twice with 608.8 and 501.9 watts, and four times with 528.2 watts. The SP configuration produces voltages of 76.64, 58.82, 58.21, and 39.56 volts individually, twice with 75.38 volts, and three times with 39.20 volts. The current follows the voltage variation. The TCT setup generates voltages of 77.62 volts individually, twice with 58.82 and 58.21 volts, and four times with 76.64 volts. The current variation also corresponds to the voltage. The data above clearly shows that SP has more diversity than TCT. Therefore, SP and TCT has GMPP diversity of 6 and 4, respectively.

Table 3 also provides the information about LMPP with different peak numbers and their frequency of occurrence in the SP and TCT configurations. This provides valuable insights into the performance of these PV array configurations under partial shading conditions. The fact that the SP configuration produces LMPP with two, three, and four peaks, each appearing three times, suggests that this configuration may not be able to track the LMPP accurately, leading to significant power losses.

Table 3 GMPP and LMPP parameters of SP and TCT configuration under various PS patterns as in Figure 3 (a) – (i)

Config.	Parameter	Pattern								
		a	**b**	**c**	**d**	**e**	**f**	**g**	**h**	**i**
SP	P_{GMPP} (watts)	608.8	528.2	501.88	477.8	405.9	405.9	405.9	389.3	389.3
	V_{GMPP} (volts)	58.82	76.64	58.21	39.56	39.20	39.20	39.20	75.38	75.38
	I_{GMPP} (amps)	10.35	6.89	8.62	12.08	10.35	10.35	10.35	5.16	5.16
	Loss	56%	62%	64%	66%	71%	71%	71%	72%	72%
	N_{LMPP}	3	2	4	2	3	4	4	2	3
		i	**e**	**a**	**b**	**d**	**f**	**h**	**c**	**g**
TCT	P_{GMPP} (watts)	669.18	608.8	608.8	528.22	528.22	528.22	528.2	501.88	501.88
	V_{GMPP} (volts)	77.62	58.82	58.82	76.64	76.64	76.64	76.64	58.21	58.21
	I_{GMPP} (amps)	8.62	10.35	10.35	6.89	6.89	6.89	6.89	8.62	8.62
	Loss	52%	56%	56%	62%	62%	62%	62%	64%	64%
	N_{LMPP}	2	2	3	2	2	2	2	4	4

On the other hand, the TCT configuration produces two peaks that appears six times, three peaks that appears only once, and four peaks that appears only twice, indicating a better ability to track the LMPP and potentially reducing power losses due to partial shading. The number of LMPP can affect the complexity of the Maximum Power Point Tracking (MPPT) algorithm. In general, a PV array with fewer LMPPs will have a simpler MPPT algorithm. This is because the algorithm only needs to track the single or limited number of LMPPs to determine the optimal operating point of the array.

In addition, both the SP and TCT configurations can have the same GMPP parameters, but with different numbers of LMPP for some PS patterns. SP configuration with PS patterns as shown in Figures 3 (e), (f), and (g) have the same GMPP parameters but different numbers of LMPP, namely 3, 4, and 4, respectively; the same goes for patterns in Figures 3 (h) and (i), with 2 and 3 LMPPs, respectively. As for the TCT configuration with PS patterns in Figures 3 (e) and (a), they have 2 and 3 LMPPs, respectively.

4.0 CONCLUSION

Simulation using nine different PS patterns with 45% shadowed area resulted in LMPP of SP configuration with 2, 3, and 4 peaks occurring three times each, resulting in total peaks of 27. On the other hand, TCT configuration provided 2 peaks occurring six times, 3 peaks occurring three times, and 4 peaks occurring twice, resulting in total peaks of 24. In terms of GMPP magnitude, the SP configuration experienced power losses ranging from 56% to 72%, generating voltage of 39.20 to 76.64 volts. The TCT configuration experienced power loss of 52% to 64%, generating voltage of 58.21 to 77.62 volts. The diversity of GMPP for the SP and TCT configurations was 6 and 4, respectively. The SP configuration had two pairs of GMPP with different numbers of LMPP, while the TCT configuration only had one pair. In conclusion, the TCT outperforms SP which is presented with the more detailed and integrated analysis concerning the efficiency and effectiveness of MPPT.

Conflicts of Interest

The author(s) declare(s) that there is no conflict of interest regarding the publication of this paper.

Acknowledgement

This research is fully supported by the LPPM – STT Duta bangsa grant. The authors fully acknowledged Sekolah Tinggi Teknologi Duta Bangsa, Bekasi, Indonesia for the approved fund which makes this important research viable and effective.

References

[1] N. A. Windarko, M. N. Habibi, B. Sumantri, E. Prasetyono, M. Z. Efendi, and Taufik. 2021. A New MPPT Algorithm for Photovoltaic Power Generation under Uniform and Partial Shading Conditions. *Energies (Basel)*. 14(2). Doi: 10.3390/en14020483.

[2] M. V. Dambhare, B. Butey, and S. V. Moharil. 2021. Solar Photovoltaic Technology: A Review of Different Types of Solar Cells and Its Future Trends. *Journal of Physics: Conference Series*. 1913(1). Doi: 10.1088/1742-6596/1913/1/012053.

[3] A. A. Desai and S. Mikkili. 2019. Modelling and Analysis of PV Configurations (Alternate TCT-BL, Total Cross Tied, Series, Series Parallel, Bridge Linked and Honeycomb) to Extract Maximum Power Under Partial Shading Conditions. *CSEE Journal of Power and Energy Systems*. 8(6). Doi: 10.17775/CSEEJPES.2020.00900.

[4] L. A. Trejos-Grisales, J. D. Bastidas-Rodríguez, and C. A. Ramos-Paja. 2020. Mathematical Model for Regular and Irregular PV Arrays with Improved Calculation Speed. *Sustainability (Switzerland)*. 12(24): 1-28. Doi: 10.3390/su122410684.

[5] L. Xu, R. Cheng, and J. Yang. 2020. A New MPPT Technique for Fast and Efficient Tracking under Fast Varying Solar

Irradiation and Load Resistance. *International Journal of Photoenergy*. 2020. Doi: 10.1155/2020/6535372.

[6] S. Amar, M. Bahich, Y. Bentahar, M. Afifi, and E. Barj. 2021. A Study of the Temperature Influence on Different Parameters of Mono-Crystalline Silicon Photovoltaic Module. *Journal of Power and Energy Engineering*. 09(06): 29-42. Doi: 10.4236/jpee.2021.96003.

[7] M. Premkumar, U. Subramaniam, T. Sudhakar Babu, R. M. Elavarasan, and L. Mihet-Popa. 2020. Evaluation of Mathematical Model to Characterize the Performance of Conventional and Hybrid PV Array Topologies under Static and Dynamic Shading Patterns. *Energies (Basel)*. 13(12). Doi: 10.3390/en13123216.

[8] M. A. Koondhar, I. A. Channa, S. Chandio, M. I. Jamali, A. S. Channa, and I. A. Laghari. 2021. Temperature and Irradiance-based Analysis the Specific Variation of PV Module. *J Teknol*. 83(6): 1-17. Doi: 10.11113/jurnalteknologi.v83.16609.

[9] S. Bounouar *et al.* 2020. Assessment of Series Resistance Components of a Solar PV Module Depending on its Temperature Under Real Operating Conditions.

[10] A. D. Dhass, Y. Prakash, and K. C. Ramya. 2020. Effect of Temperature on Internal Parameters of Solar Cell. *Materials Today: Proceedings*. 33: 732-735. Doi: 10.1016/j.matpr.2020.06.079.

[11] M. Yesilbudak. 2021. Parameter Extraction of Photovoltaic Cells and Modules using Grey Wolf Optimizer with Dimension Learning-based Hunting Search Strategy. *Energies (Basel)*. 14(18). Doi: 10.3390/en14185735.

[12] S. R. Pendem, S. Mikkili, S. S. Rangarajan, S. Avv, R. E. Collins, and T. Senjyu. 2021. Optimal Hybrid PV Array Topologies to Maximize the Power Output by Reducing the Effect of Non-uniform Operating Conditions. *Electronics (Switzerland)*. 10(23). Doi: 10.3390/electronics10233014.

[13] A. Y. Appiah, X. Zhang, B. B. K. Ayawli, and F. Kyeremeh. 2019. Review and Performance Evaluation of Photovoltaic Array Fault Detection and Diagnosis Techniques. *International Journal of Photoenergy*. Hindawi Limited. Doi: 10.1155/2019/6953530.

[14] S. R. Pendem, S. Mikkili, S. S. Rangarajan, S. Avv, R. E. Collins, and T. Senjyu. 2021. Optimal Hybrid PV Array Topologies to Maximize the Power Output by Reducing the Effect of Non-uniform Operating Conditions. *Electronics (Switzerland)*. 10(23). Doi: 10.3390/electronics10233014.

[15] K. Rajani and T. Ramesh. 2022. Reconfiguration of PV Arrays (T-C-T, B-L, H-C) Considering Wiring Resistance. *CSEE Journal of Power and Energy Systems*. 8(5): 1408-1416. Doi: 10.17775/CSEEJPES.2020.06930.

[16] J. Gosumbonggot and G. Fujita. 2019. Global Maximum Power Point Tracking under Shading Condition and Hotspot Detection Algorithms for Photovoltaic Systems. *Energies (Basel)*. 12(5): Doi: 10.3390/en12050882.

[17] T. Sutikno, A. Pamungkas, G. Pau, A. Yudhana, and M. Facta. 2022. A Review of Recent Advances in Metaheuristic Maximum Power Point Tracking Algorithms for Solar Photovoltaic Systems Under the Partial-Shading Conditions. *Indonesian Journal of Science and Technology*. 7(1): 131-158. Doi: 10.17509/ijost.v7i1.45612.

[18] A. Giyantara, Wisyahyadi, R. B. Rizqullah, and Y. T. Kusuma Priyanto. 2021. Analysis of Partial shading Effect on Solar Panel Power Output. *Journal of Physics: Conference Series*. 1726(1). Doi: 10.1088/1742-6596/1726/1/012022.

[19] C. Huang and L. Wang. 2018. Simulation Study on the Degradation Process of Photovoltaic Modules. *Energy Convers Manag*. 165: 236-243. Doi: 10.1016/j.enconman.2018.03.056.

[20] A. Bennani-Ben Abdelghani and H. ben Attia Sethom. 2020. Modeling PV Installations under Partial Shading Conditions. *SN Appl Sci*. 2(4). Doi: 10.1007/s42452-020-2458-0.

[21] P. Manoharan *et al.* 2021. Improved Perturb and Observation Maximum Power Point Tracking Technique for Solar Photovoltaic Power Generation Systems,".*IEEE Syst J*. 15(2): 3024-3035. Doi: 10.1109/JSYST.2020.3003255.

[22] C. Prakash Meena. 2018. Study of Maximum Power Point Tracking (MPPT) in Solar Panels. *International Journal of Science and Research*. Doi: 10.21275/ART20198530.

[23] M. A. Abo-Sennah, M. A. El-Dabah, and A. E. B. Mansour. 2021. Maximum Power Point Tracking Techniques for Photovoltaic Systems: A Comparative Study. *International Journal of Electrical and Computer Engineering*. 11(1): 57-73. Doi: 10.11591/ijece.v11i1.pp57-73.

[24] S. D. Al-Majidi, M. F. Abbod, and H. S. Al-Raweshidy. 2018. A Novel Maximum Power Point Tracking Technique based on Fuzzy Logic for Photovoltaic Systems. *Int J Hydrogen Energy*. 43(31): 14158–14171. Doi: 10.1016/j.ijhydene.2018.06.002.

[25] A. S. Mahdi, A. K. Mahamad, S. Saon, T. Tuwoso, H. Elmunsyah, and S. W. Mudjanarko. 2020. Maximum Power Point Tracking Using Perturb and Observe, Fuzzy Logic and ANFIS. *SN Appl Sci*. 2(1). Doi: 10.1007/s42452-019-1886-1.

[26] R. K. Pachauri. 2020. Investigation on SP and TCT Photovoltaic Array Configurations under Obscured Shading Conditions. *7th IEEE Uttar Pradesh Section International Conference on Electrical, Electronics and Computer Engineering, UPCON 2020*. Doi: 10.1109/UPCON50219.2020.9376510.

[27] R. G. Vieira, F. M. U. de Araújo, M. Dhimish, and M. I. S. Guerra. 2020. A Comprehensive Review on Bypass Diode Application on Photovoltaic Modules. *Energies*. 13(10). Doi: 10.3390/en13102472.

[28] F. Belhachat and C. Larbes. 2015. Modeling, Analysis and Comparison of Solar Photovoltaic Array Configurations under Partial Shading Conditions. *Solar Energy*. 120: 399-418. Doi: 10.1016/j.solener.2015.07.039.